The role of field spectroscopy in airborne sensor calibration: an example of the NERC CASI

E.M. ROLLIN, E.J. MILTON and K. ANDERSON

NERC EPFS, Department of Geography, University of Southampton, UK. email: ***epfs@soton.ac.uk***

Abstract

This paper reports on a preliminary experiment to undertake in-flight radiance calibration validation (cal-val) of the NERC CASI. The approach involved comparing CASI radiance values of a single, well-characterised target with synchronised measurements of target radiance obtained at the ground with a calibrated spectroradiometer. CASI data were obtained at two altitudes: 853m and 3109m, in spatial mode using the default vegetation band-set. For the lower altitude image, there was very good agreement between the image and ground-measured radiance especially in bands 4 to 6 (670nm-710nm). An atmospheric correction based on the multi-height image data significantly improved the image versus ground comparison for bands 1 to 3, where scattering dominates. However, the correction performed less well for the two NIR bands coincident with the atmospheric absorption regions (band 9 at 762nm and band 13 at 940nm). For the asphalt target, estimating radiance from spectral reflectance measured post-flight combined with spectral irradiance measured during the flights was found to be a viable alternative to measuring radiance. Overall, the results suggest the method could be developed further to provide in-flight calibration validation of the CASI to supplement or replace the mid-season laboratory calibration.

1. Introduction

In remote sensing, the radiometric calibration function transforms the sensor response from Digital Number (DN) to System International (SI) units of spectral radiance (mW m-2 sr-1 nm-1). This makes the measurements independent of the sensor and is prerequisite to relating the signal received at the sensor to some geophysical characteristic of the object viewed (Thome 2001, Rigollier *et al.* 2002). Laboratory-based methods provide the most accurate approach to absolute radiometric calibration and are typically performed against a traceably calibrated light source, such as an integrating sphere or irradiance lamp (Slater 1980). For a linear sensor, ratioing the DN output from the sensor with the value of an accurately known uniform radiance field at its entrance pupil yields the calibration coefficient (Dinguirard and Slater 1999), based on the following equation:

$$X = AL \qquad \textit{eq. 1}$$

where, X is the digital output of the sensor, L the radiance at the entrance slit of the instrument and A is the absolute radiometric calibration coefficient to be determined (Schott, 1997, Schowengerdt, 1997, Dinguirard and Slater, 1999).

For satellite-borne sensors, laboratory radiometric calibration is performed pre-launch and monitoring of the sensor performance continues post-launch, since the accuracy of the pre-flight calibration may be compromised by in-operation disturbances (Dinguirard and Slater, 1999). In-flight calibration-validation (cal-val) procedures for satellite sensors are widely documented in the literature. They include: i) the measurement of a secondary light source housed on the platform (Dinguirard and Slater, 1999); ii) direct measurement of the solar exoatmospheric spectral irradiance (Slater 1985), and iii) independent 'vicarious calibration' pathways utilising measurements of specific ground targets (Abdou *et al.,* 2001, Arai, 2001, Secker *et al.,* 2001, Slater *et al.,* 1996, Teillet *et al.,* 2001).

For airborne sensors the laboratory radiometric calibration is repeated at regular intervals and usually necessitates the removal of the sensor from the flying platform. Methods of in-flight cal-val for airborne scanners are not widely documented with the implication that such procedures are not generally adopted as operational. For airborne sensors, unlike satellite systems, measuring the exoatmospheric spectral irradiance is not feasible. A recognised disadvantage of secondary light sources is that they provide a vastly different colour temperature with no fine spectral structure compared to sunlight (Kieffer and Wildey, 1996). The most appropriate approach for airborne systems, is to use cal-val procedures based on accurately calibrated spectral measurements made simultaneously at the ground (Slater *et al*., 1987, Dinguirard and Slater, 1999). This approach has the advantage that the illumination conditions are consistent with those under which data are routinely collected.

Field spectroscopy underpins the quantitative analysis of airborne remotely-sensed data through a number of widely-used techniques, including provision of spectral ground data for image classification (Ferrier, 1999, Thomas *et al.,* 2003), and for empirical atmospheric scene correction (Smith and Milton, 1999, Moran *et al.,* 2001, Karpouzli and Malthus, 2003). Field spectroradiometry has been used for vicarious calibration of satellite sensors (e.g. Teillet, et al., 2001), but for vicarious calibration of airborne sensors the method is often based on post-flight measurements of surface reflectance (e.g. Secker *et al.,* 2001). The cal-val procedure reported in this paper relies on using simultaneous ground-based spectral measurements obtained with calibrated field spectroradiometers to provide an independent validation of the radiometric calibration of an airborne hyperspectral sensor.

The CASI (Compact Airborne Spectrographic Imager) is an airborne hyperspectral scanner, owned and operated by the UK Natural Environment Research Council (NERC). CASI is calibrated to radiance in a laboratory procedure defined by the scanner manufacturers, ITRES Instruments (Riedmann and Rollin, 2000). The calibration is performed at the EPFS laboratory against a Hoffman LS-64-8D integrating sphere. This primary radiance standard is calibrated annually at the UK National Physical Laboratory (NPL), and laboratory calibration of the CASI is typically performed two or three times per year.

Laboratory calibration of the sensor requires removal and refitting the system from the aircraft, which is disruptive to the flying schedule, especially when the

calibration is mid-season. The potential benefits of an in-flight calibration check, which could supplement or even replace the mid-season laboratory calibration, are considerable. An in-flight procedure offers additional advantages in the case of the NERC CASI, matching the conditions of data collection and enabling monitoring of the radiometric performance of the sensor between the laboratory calibrations.

The aim of this experiment was to develop a repeatable methodology for in-flight cal-val of the CASI sensor and explore its potential for providing an 'independent calibration pathway' (Bruegge, 2001) which might replace the present mid-season laboratory calibration of the CASI with a field calibration method. The method was based on simultaneous measurements of spectral radiance of a calibration target at the ground, using a calibrated spectroradiometer from the NERC Equipment Pool for Field Spectroscopy (EPFS) following the method proposed by Thome (1999). These data were with radiometrically calibrated image data from CASI from a simultaneous, low altitude overpass of the test site. Three specific objectives of the experiment were:

i) To make a direct comparison of the radiance of a well-characterised, uniform target measured by the CASI with the radiance measured simultaneously at the ground with the spectroradiometer.

ii) To evaluate whether estimating the target radiance based upon the target spectral reflectance and spectral irradiance measured at the time of the flight offered a viable alternative to measuring target radiance directly.

iii) To use multi-height image data to produce an atmospheric correction of the image data to further extend the comparison of the CASI radiance to that measured at the ground, according to the method proposed by Steven and Rollin (1986).

2. Measurement Methodology

2.1 The Calibration Site

The experiment took place at Thorney Island (Figure 1), a disused airfield in West Sussex, which has been the subject of calibration work over several years (Milton *et. al.* 1996, Lawless *et. al.* 1998). Data from previous NERC flights over Thorney Island have demonstrated its suitability as a remote sensing calibration site. The main N-S runway is composed of asphalt and has a spatially uniform spectral reflectance. The runway also includes two other surfaces, a darker bitumen area at the northern end (Thorney Northern Asphalt - TNA) and an area of square concrete slabs at the southern end (Thorney Southern Concrete - TSA). Immediately adjacent to the southern end of the main runway is an area of short grass, which is regularly mown (Thorney Southern Grass - TSG). This has also been found useful as a calibration target. This experiment focused on the most uniform of the four calibration sites, the Thorney Southern Asphalt (TSA).

Figure 1: Thorney Island Calibration Site identifying the four calibration targets: TNA - Thorney Northern Asphalt; TSA - Thorney Southern Asphalt; TSC - Thorney Southern Concrete and TSG - Thorney Southern Grass.

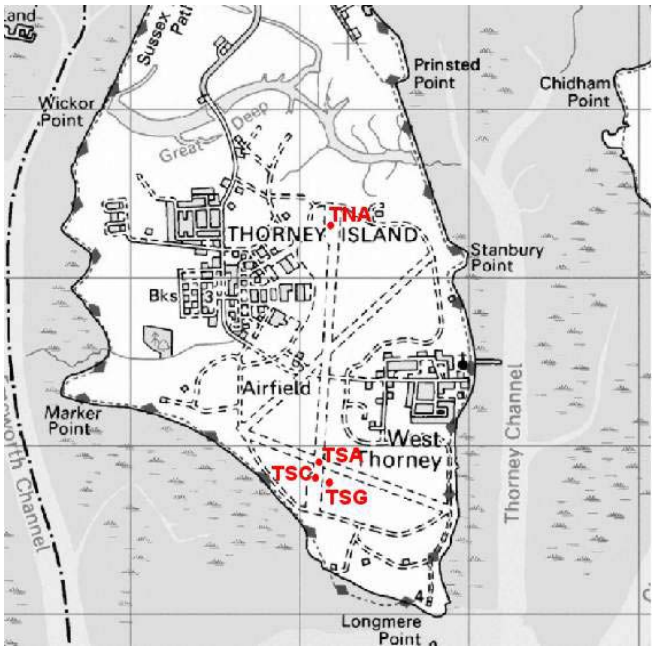

2.2 Thorney Island - Ground Data

Table 1 summarises the field measurements obtained during the CASI over-flights on 24 July 2001.

Table 1: Summary of ground measurements

Quantity	**Sensor**	**Wavelength Range**	**Map Code**	**Sampling Interval**
Asphalt (TSA) Radiance	GER1500 (3° field-of-view)	VIS-NIR (300-100nm)	TSA	30 seconds
Global Spectral Irradiance	ASD FieldSpec Pro (with cosine corrected receptor fitted)	VIS-SWIR (300-2400nm)	E	30 seconds
Global Broadband Irradiance	Delta-T ES2 Energy sensor	VIS-NIR (400-1100nm)	E	5 seconds
Global and Diffuse Quantum flux (PAR)	Delta-T BF2 Sunshine sensor	PAR (400-700nm)	E	5 seconds
Direct Irradiance (5 bands)	Microtops II	Bands at 440, 675, 870, 936 and 1020nm	E	As required
Aerosol Optical Thickness (AOT) (5 bands)				

The asphalt radiance was measured at the intersection of the N-S and E-W runways, using the GER1500 spectroradiometer. This sensor was tripod mounted and operated in automatic repetitive sampling mode to measure and store the data without the need for operator involvement so that the area of asphalt was free of personnel during the CASI over-flights. The objective of these measurements was to obtain the radiance of the asphalt target synchronous with the CASI data. The GER1500 was calibrated to radiance in the EPFS laboratory against the primary radiance standard, a Hoffman LS-64-8D integrating sphere.

The ASD FieldSpec Pro fitted with a cosine corrected hemispherical diffuser was used to measure incident global spectral irradiance throughout the period of over-flights. The instrument was positioned 10m east of the asphalt area together with the other broadband irradiance sensors. The ASD FieldSpec Pro was calibrated to irradiance in the EPFS laboratory against the in-house irradiance standard, an OL FEL-U 1000w lamp, which is calibrated annually at the NPL.

Both the spectroradiometers were warmed up for 90 minutes before measurements commenced. Data from both spectroradiometers were collected in raw DN format and processed to radiance or irradiance using the EPFS post-processing software and the appropriate radiometric calibration for that sensor.

After the CASI flights were completed the ASD FieldSpec Pro was used to measure the spectral reflectance of the asphalt target and derive the mean spectral reflectance appropriate to that day.

2.3 Thorney Island - CASI data

CASI data were collected early on the morning of 24 July 2001. Two N-S overpasses of the Thorney Site were made at different altitudes, both centred on the main N-S runway (table 2).

Table 2: CASI data of Thorney Island 24 July 2001.

	Direction	Altitude	Mode	Bandset	GMT (start)
Higher Flight line Ref: c205023	N-S	3109m/ 10200ft	Spatial	Default Vegetation	08:46:40
Lower Flight line Ref: c205033	N-S	853m/ 2800ft	Spatial	Default Vegetation	08:56:54

Figure 2 shows that after 09:00 GMT the sky conditions deteriorated, although both images were acquired under cloud-free conditions (figure 3). The early morning timing of the flights meant that there was a systematic increase in irradiance between the time of the two images due to the rapidly increasing solar elevation angle. Despite the short time interval between the two flights it was necessary to correct the radiance data from one image relative to the other when data from the two images were directly compared. Figure 3 indicates that the change in broadband global irradiance between the two images was of the order of 7-8%. For this work, however, a spectrally dependent irradiance correction was used based on the spectral irradiance measurements obtained with the ASD FieldSpec Pro. The corrections were consistent with the spectral radiance variation recorded with the GER1500 for the asphalt site over that time period, and with the global irradiance data from the other sensors.

Figure 2: Broadband Global Irradiance at Thorney Island, 24 July 2001

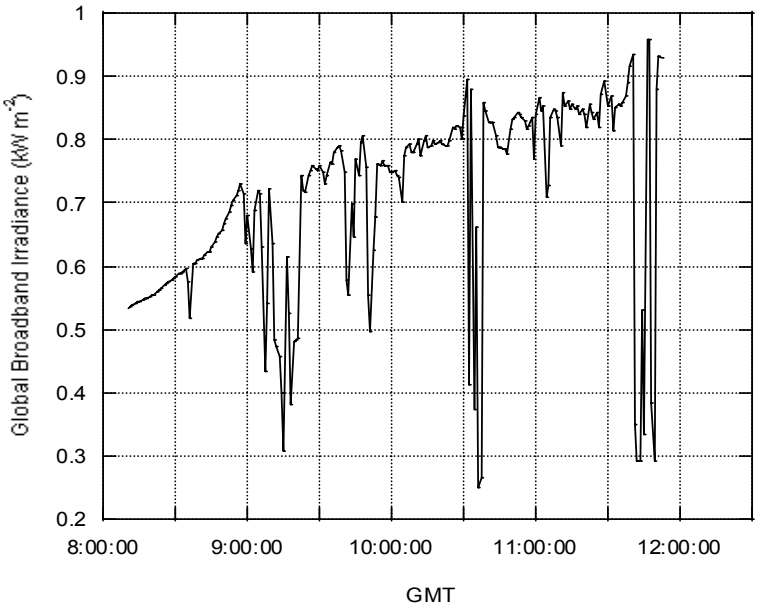

The CASI image data were provided calibrated to radiance units (*level 1b*). The computer program *AZGcorr* was then used to extract the geometric correction information, which was subsequently applied to the data to create a *level 3a* image. At this level, the data are corrected for aircraft attitude variation and rectified to the British National Grid. Mean radiance was extracted for the asphalt target area on the images from both altitudes. In both cases the target was within the central 20 pixels of the image so that the view angle deviated by less than 2% from the nadir. Subsequently, mean radiance of three additional targets was extracted from both images (see section 4). The time of the images was obtained from navigation data embedded in the level 1b HDF file. Table 3 summarises the centre wavelengths and bandwidth of the CASI vegetation band-set.

3. Analysis and results

3.1 Image vs ground radiance comparison

The first stage of the analysis was to compare directly the simultaneous ground and image radiance measurements of the asphalt target, for both overpasses (figures 4 and 5).

Table 3: CASI Spatial Mode Default Vegetation Band-set

Band	Centre wavelength (nm)	Nominal Bandwidth FWHM (nm)
1	450.18	20
2	490.29	20
3	552.32	10
4	670.06	10
5	700.63	10
6	710.19	10
7	740.83	10
8	750.41	6
9	762.86	4
10	781.08	10
11	820.41	8
12	865.49	10
13	940.2	10

Figure 3: Broadband Global Irradiance during the CASI overflights

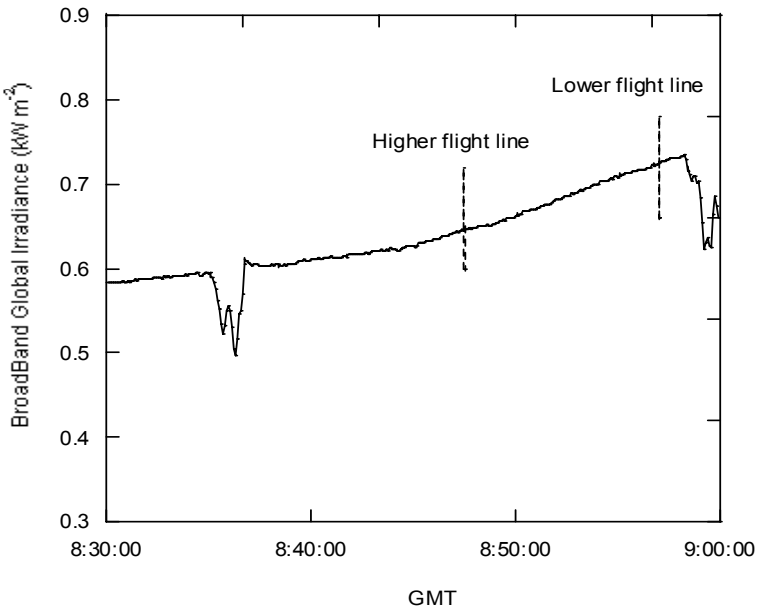

Figure 6 shows that there is good agreement between the ground measured radiance and the CASI values for the lower altitude image. In fact, for bands 4, 5 and 6 the radiance values from the 853m image are within 1% of the values measured at the ground. For the higher altitude image the asphalt radiance exceeds the ground measured value in all bands except band 13, with the difference being approximately 2% in bands 4 to 6 but 30% in band 1. This is consistent with increased scattering at shorter wavelengths through the greater depth of atmosphere.

The similarity of radiance measured at both altitudes in bands 4 to 6 (650nm to 720nm) suggests a relatively small atmospheric effect at these wavelengths so that direct comparison of the CASI and ground-measured radiance constitutes a viable approach.

Figure 4: Radiance of the asphalt target from the CASI at the Higher flight line, (3109m) (—●—) and at the ground (——).

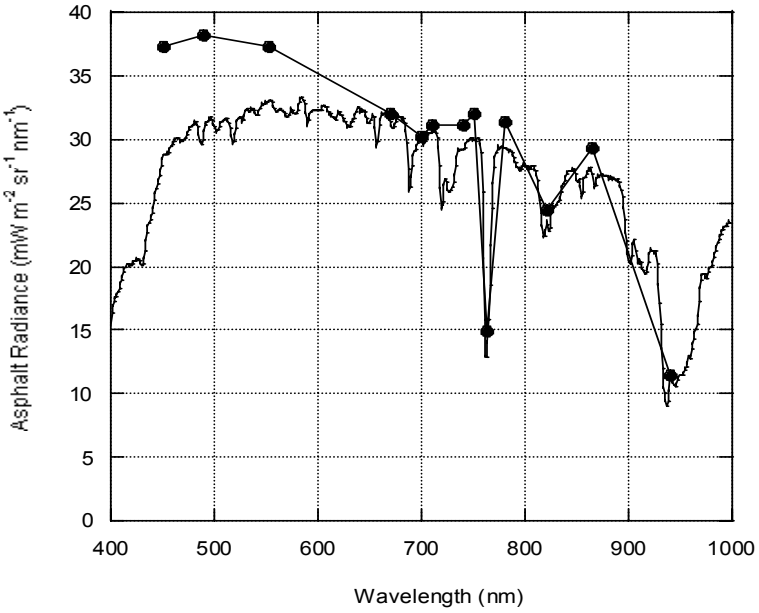

Figure 5: Radiance of the asphalt target from the CASI Lower flight line (853m) (—●—) and at the ground (——).

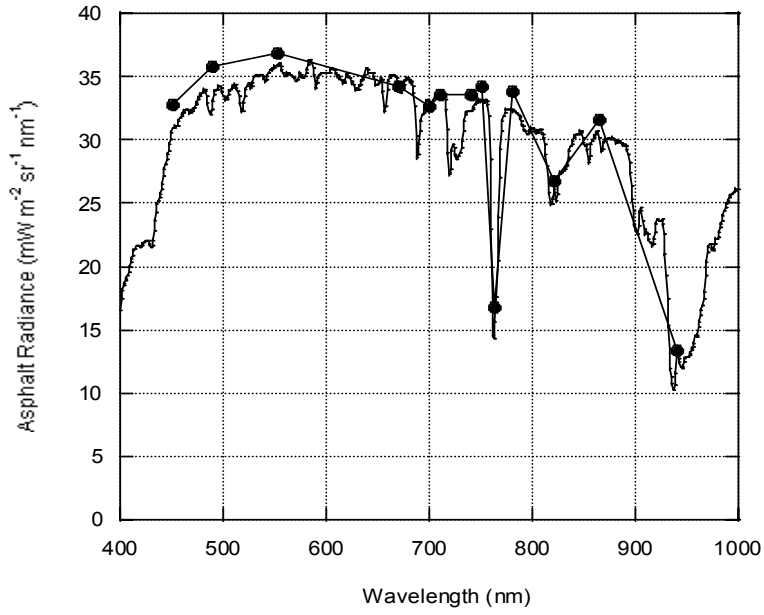

Figure 6: Ratio of CASI Radiance to GER1500 Radiance

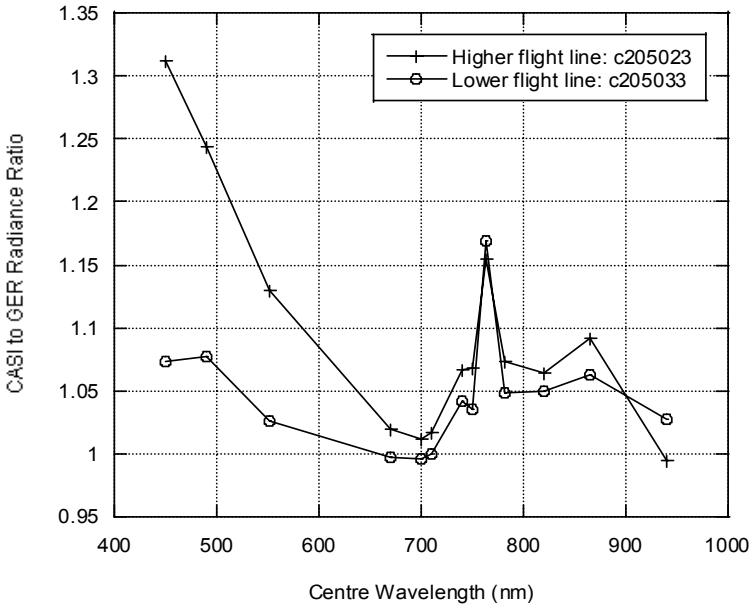

3.2 Radiance measurements vs radiance estimates

The second stage of the work examined the possibility of deriving the radiance of the asphalt target at the time of the over-flights, from reflectance of the target combined with synchronous measurements of spectral irradiance. The rationale behind this was to maximise the potential application of the in-flight procedure, since it is logistically less demanding to measure irradiance during the image data acquisition than to measure target radiance directly. If the target radiance can be obtained from simultaneous irradiance measurements and the target spectral reflectance measured close to that time, the method might more easily be made operational, with scheduled and even opportunistic calibration runs throughout the flying programme.

In this case the mean of the reflectance spectra for the asphalt measured with the ASD FieldSpec Pro post-flight was used (figure 7). The mean spectral reflectance was combined with the spectral irradiance measured at the time of the overflight to estimate radiance for the asphalt as:

$$\rho\lambda \bullet E\lambda / \pi \qquad \textit{eq. 2}$$

where, ρ is the reflectance of the asphalt and E is the global irradiance incident on a level surface at the time of the overpass.

Figure 8 confirms the good agreement between the estimated and measured radiance for the asphalt target at the time of lower flight line. The same was true for the estimated and measured radiance of the target at the time of the higher flight line. For the lower flight line, the percentage difference between estimated and measured radiance is within 3% for most wavelengths (figure 9) although there are three wavelength regions where the difference is greater.

Between 400nm and 450nm the difference reaches 10% and at the 762nm and 940nm atmospheric absorption bands the difference. In all cases the main cause of this is the reduced signal-to-noise (SNR) of the data because of the low incident flux. In addition, SNR in the 400-450nm region is affected by decline in detector sensitivity which occurs towards the lower limit of the detector range. For the absorption bands, especially the narrower 762nm feature, slight discrepancies between the sensor spectral response and calibration inaccuracies contribute to the greater difference between estimated and measured, illustrating the potential difficulty in inter-relating data from different sensors across these regions.

Both the estimated and measured spectra were then resampled by linear interpolation to the centre wavelengths of the CASI bands. The percentage difference between the estimated and measured radiance at the time of both images is shown in figure 10. This reveals good agreement for all bands with the exception of bands 9 and 13. The much greater difference between the estimated and measured radiance for CASI bands 9 and 13 is due to their coincidence with the atmospheric absorption bands of oxygen and water vapour respectively and the fact that the two sensors have slightly different spectral characteristics over this region. Where the flux being measured changes markedly with wavelength even very slight discrepancies between the spectral sampling characteristics of the two sensors can be important. This illustrates that in regions of strong atmospheric absorption the comparison of spectral data from multiple sources is extremely sensitive to the sensor wavelength characteristics.

Despite the problem with bands 9 and 13, it is concluded that the estimating radiance by this method offers a valid alternative to measuring radiance directly, and further work is in progress to extend the technique using irradiance measured with alternative sensors operating in discrete spectral bands.

Figure 7: Mean Spectral reflectance of the asphalt target

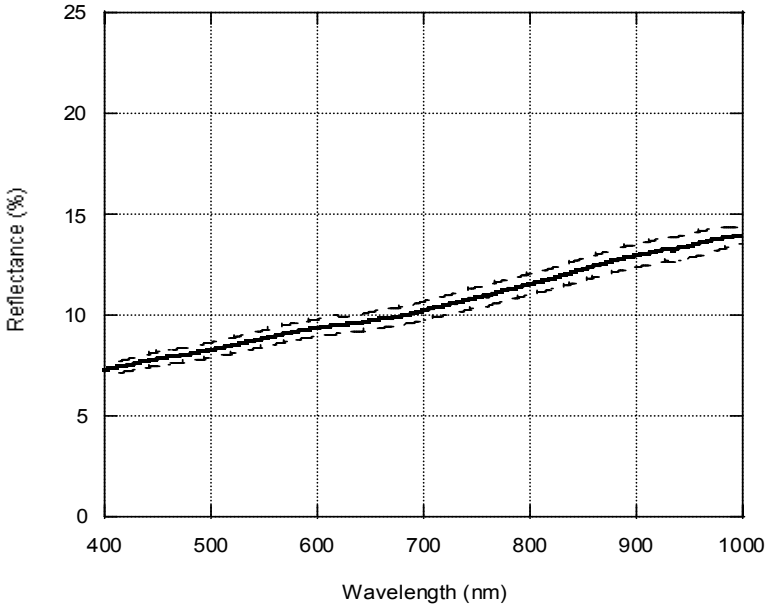

Figure 8: Measured and Estimated Radiance of the Asphalt target

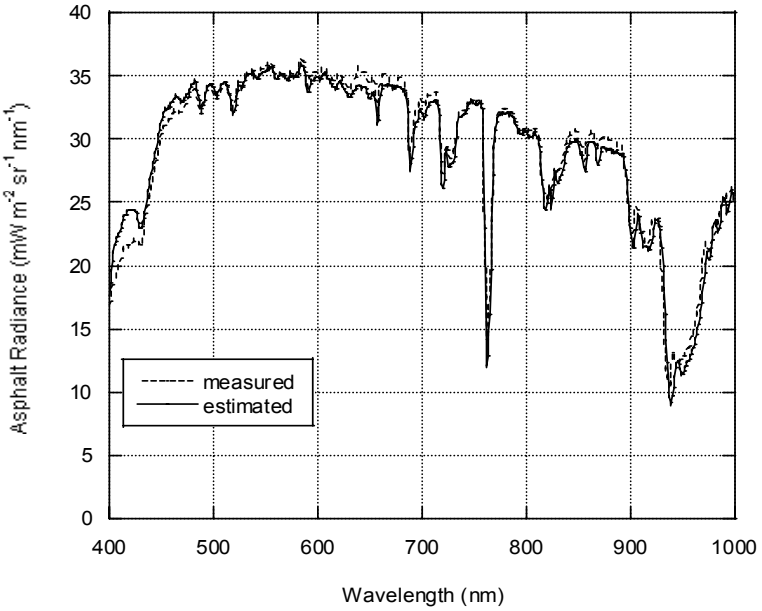

Figure 9: Percentage difference between the estimated and measured radiance of the asphalt target for the Lower flight line.

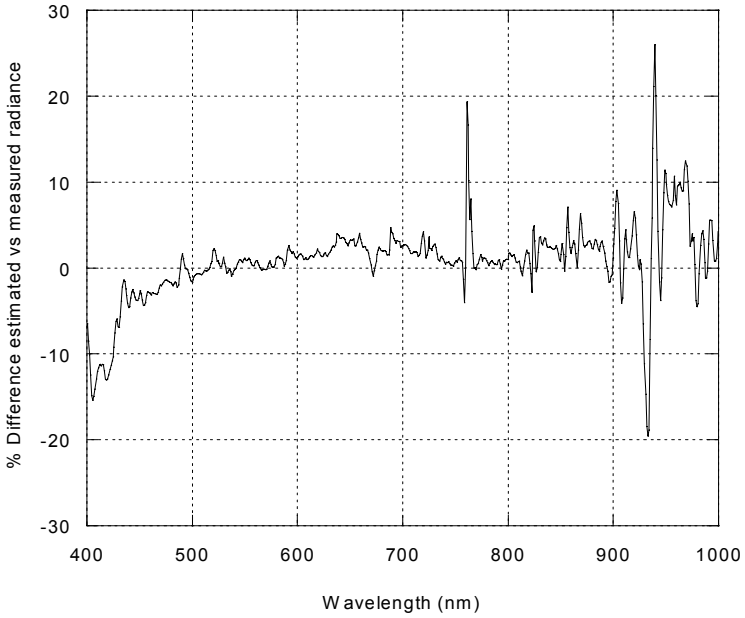

Figure 10: Percentage difference between the estimated and measured radiance of the asphalt target at the time of the CASI over-flights

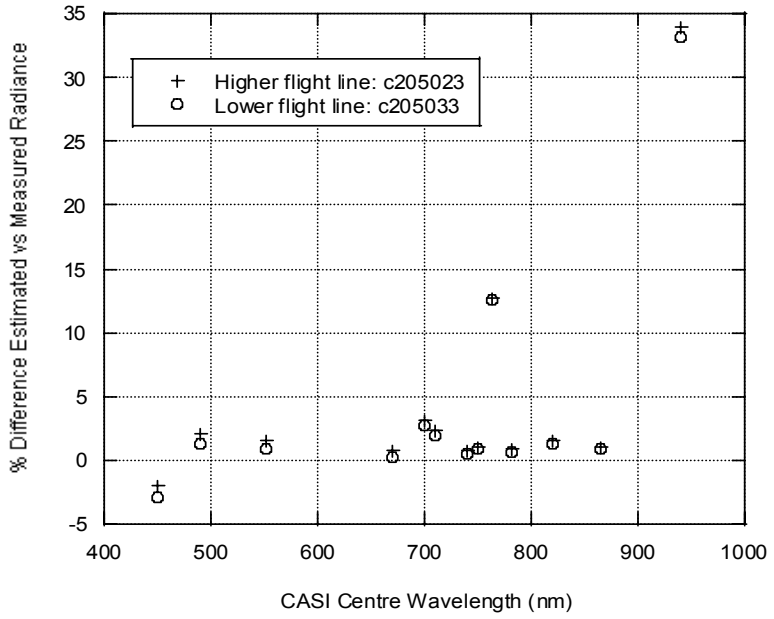

3.3 Applying an atmospheric correction using the multi-height data

The direct comparison of the image and ground radiance for the asphalt target ignores the effect of the atmosphere. Two methods of correcting for the atmosphere using the multi-height data were examined. The first is a simple extrapolation of the asphalt radiance based on the data from the two altitudes, to the ground. The second uses a multi-height inversion model to derive atmospheric transmission and path radiance values for the layer of atmosphere between the two over-flights. These parameters are then applied as corrections to the image radiance to predict the ground radiance of the asphalt surface at the time of each flight line.

The methods are described in more detail below and results from both are compared in the subsequent section.

Method 1 - Simple Extrapolation

This method uses the CASI radiance data for the asphalt target from the two heights to extrapolate the radiance at zero altitude. Firstly, a time correction was applied to correct the radiance from the Higher flight line to the time of the Lower flight line, as explained in section 2.3. Then, the time-corrected radiance for the asphalt from the two images was plotted against height (figure 11). Assuming a linear fit and extrapolating to zero altitude yields the zero radiance as the ordinate intercept.

The value retrieved is the radiance at the time of the lower flight line (i.e. the reference time to which the earlier image data were standardised). Applying

the time correction in reverse yields the extrapolated value at the ground for the time of the higher flight line.

Method 2 - Multi-height model

In the multi-height model, atmospheric transmission and path radiance were extracted by applying an inversion model to the radiance data for several targets measured at two altitudes (Steven and Rollin, 1986). The general multi-height model for the nadir view at a fixed solar azimuth angle can be written:

$$L_{h\lambda} = L_{l\lambda} \bullet T_{\lambda} + Rp_{\lambda} \qquad \textit{eq. 3}$$

Where, L_h and L_l are the radiance at the higher and lower altitude respectively, T is the transmission and Rp the path radiance for the layer. Because the relationship is linear, plotting the radiance at the higher altitude against that at the lower altitude allows the atmospheric transmission to be obtained directly as the slope of the line. The path radiance is derived from the intercept.

The model applies to monochromatic radiation since it assumes Beer's law for attenuation (also known as the Bouguer-Lambert law) holds, so it may not apply to broader spectral bands where attenuation varies significantly across the band. Applying the model to the multi-height radiance data assumes the radiation field at the surface to be uniform and the target sites located in the centre of the image/sensor array, so that the nadir view is maintained. The sites should also cover a range of albedo.

The procedure was performed on the CASI data using four sites: the asphalt runway (TSA), the area of concrete (TSC) and an area of short mown grass (TSG), plus a roof area to the north of the image.

Figure 11: Extrapolating the multi-height radiance data to the ground in CASI bands 1, 3 and 10.

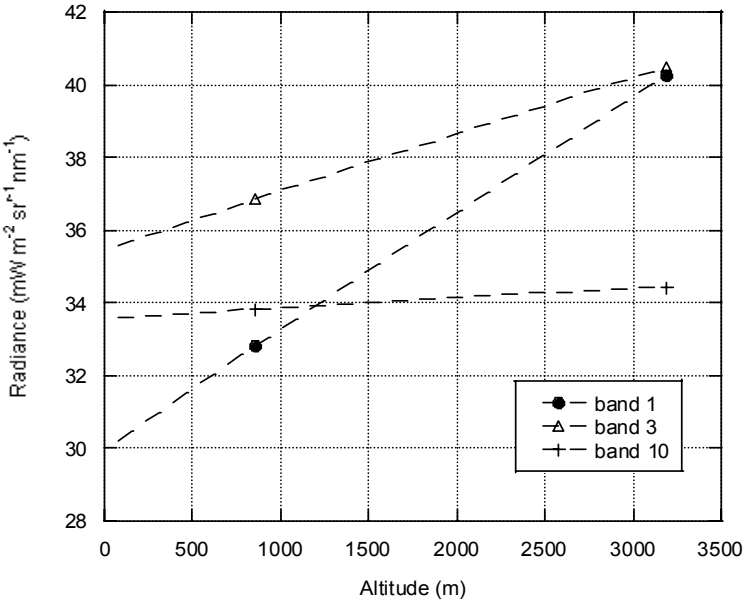

Figure 12: Multi-height inversion model to extract atmospheric transmission and path radiance - CASI band 3

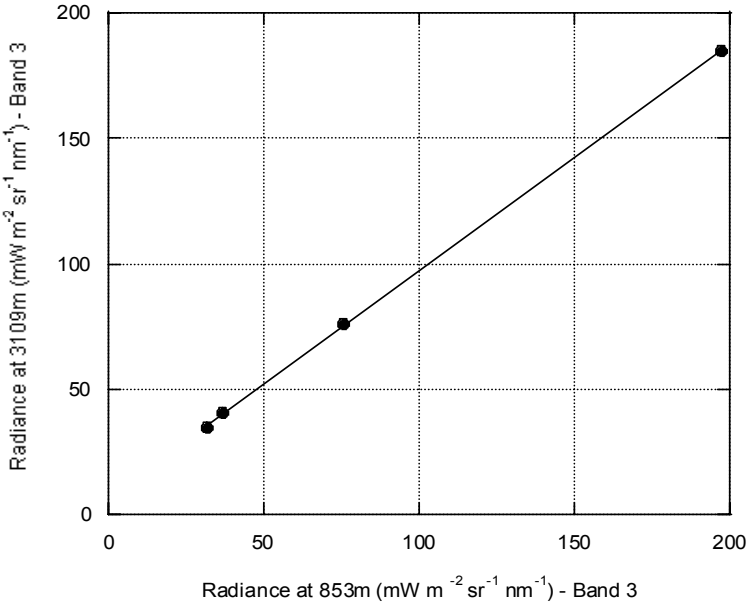

As with the simple method, the extracted radiance values from the higher flight line were adjusted to account for the change in irradiance between the two images. Figure 12 shows an example of how the multi-height method was applied to the data from band 3. Transmission and path radiance values were then obtained for each band for the (nominally) 1km to 3km layer between the two images and then normalised per 1km of atmosphere (table 4).

In order to predict the ground radiance at the time of each image, transmission and path radiance values for the lowest layer of atmosphere were obtained. Transmission for the lowest layer (the ground to 853m) was assumed to be the same per unit depth as for the (nominal) 1km-3km layer and a value for the 853m was calculated. Path radiance for the lowest layer was obtained as the equivalent for 853m of atmosphere attenuated by the transmission value for the lowest 853m layer. The transmission and path radiance values were applied to the asphalt radiance data from each image to predict the ground radiance of the target at that time by:

$$L_{0\lambda} = (L_{h\lambda} - Rp^{t}_{\lambda}) / T^{t}_{\lambda} \qquad \textit{eq. 4}$$

Where, $L_{0\lambda}$ is the radiance predicted at the ground, $L_{h\lambda}$ is the radiance at altitude, Rp^{t}_{λ} and T^{t}_{λ} are the total path radiance and transmittance values.

Table 4: Transmission (T) and Path Radiance (Rp) derived from multi-height inversion model

Band	Wvl (nm)	Slope	Intercept	T Km^{-1}	Rp Km^{-1}
1	450.18	0.8837	12.32	0.9467	5.46
2	490.29	0.8972	10.17	0.9531	4.51
3	552.32	0.9108	6.74	0.9594	2.99
4	670.06	0.9341	2.89	0.9702	1.28
5	700.63	0.9290	2.71	0.9679	1.20
6	710.19	0.9335	2.59	0.9700	1.15
7	740.83	0.9220	3.63	0.9646	1.61
8	750.41	0.9346	2.99	0.9705	1.33
9	762.86	0.8909	1.22	0.9501	0.54
10	781.08	0.9277	3.53	0.9673	1.56
11	820.41	0.9026	3.04	0.9556	1.35
12	865.49	0.8892	5.35	0.9493	2.37
13	940.2	0.8079	2.24	0.9098	0.99

Comparison of results

Figures 13 to 16 summarise the results of both methods of correction. Results of the simple extrapolation method are referred to as *Multi-Ht1,* and those from the multi-height inversion method are referred to as *Multi-Ht2*. Figures 13 and 14 compare the radiance predicted at the ground from both methods with the ground measured radiance, for the higher and lower flight line respectively. Both methods yield very similar ground radiance values especially for bands 1 to 6.

Figure 13: Comparison of CASI., ground measured and image corrected radiance of the asphalt target for the Higher flight line.

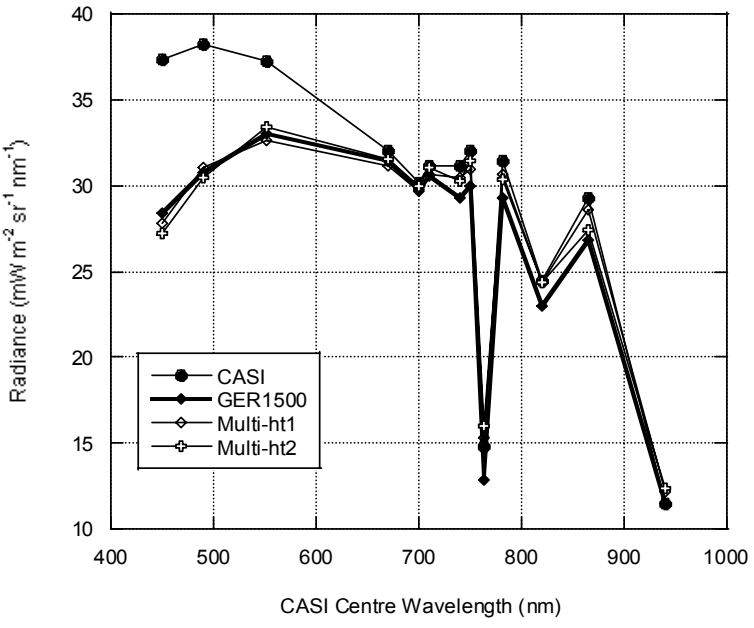

Figures 15 and 16 show the percentage deviation of the predicted value compared with ground measured. As might be expected, both methods of correcting for the atmosphere perform best for the shorter wavelength bands where scattering dominates. For bands 2 to 6, either method brings the predicted radiance to within 2-3% of the ground-measured value. For band 1 the simple extrapolation yields a slightly better result than the multi-height method, predicting the asphalt radiance to within 5% of the measured value. At longer wavelengths, bands 9 and 13 are problematic and neither method of correction performs well. This is because of their positioning in wavelength regions of strong atmospheric absorption (by oxygen and water vapour respectively) where the signal-to-noise ratio (SNR) of the measurements is reduced. For the other NIR bands (7, 8 and 10 to 12) the predicted radiance is closer than the raw data to the measured radiance although in some cases the improvement is only slight.

Both corrections perform better on data from the lower altitude, which suggests that both may be underestimating the effect of the atmosphere between 1km and 3km. However, a similar effect could arise due to uncertainty in the time correction applied to the image data in both cases. The sensitivity of the multi-height atmospheric correction method to the time correction has been pointed out in earlier work (Steven and Rollin, 1986). One future option might be to use the CASI ILS data to derive the irradiance correction provided that the effect of aircraft attitude variation can be successfully removed (Choi, 2002).

Figure 14: Comparison of CASI., ground measured and image corrected radiance of the asphalt target for the Lower flight line.

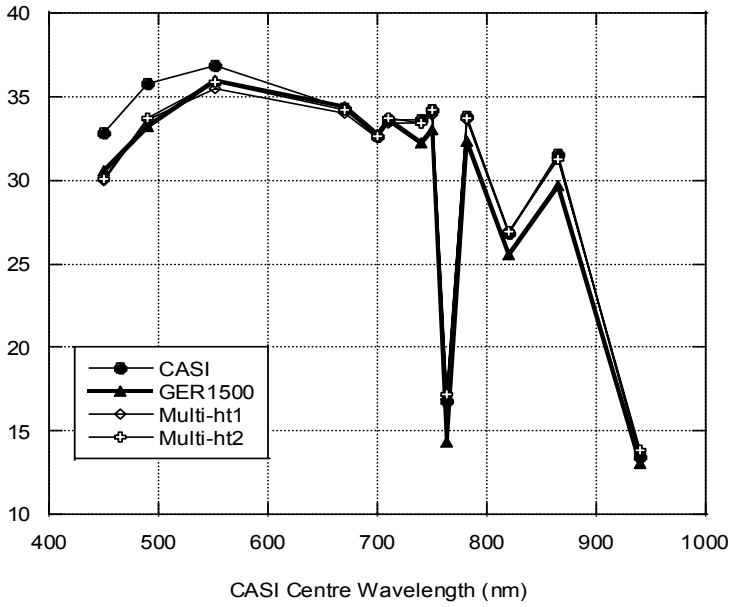

Figure 15: Percentage difference between the CASI derived and the ground measured radiance of the asphalt target for the Higher flight line.

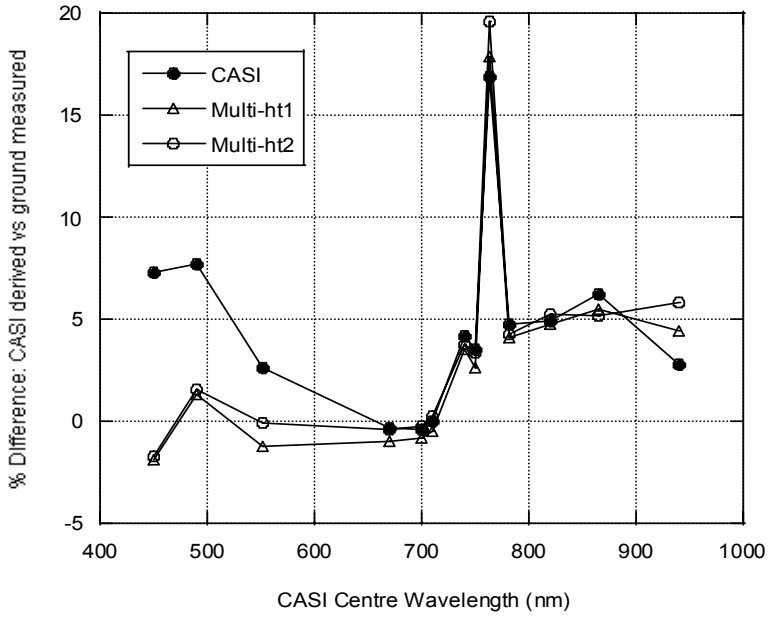

Figure 16: Percentage difference between the CASI derived and the ground measured radiance of the asphalt target for the Lower flight line.

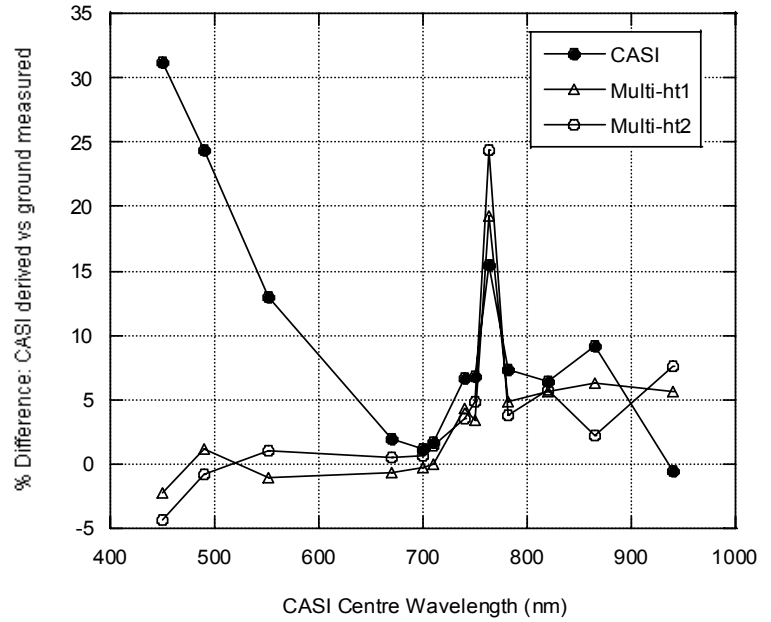

4. Conclusions

This project focused on the use of a single well-characterised target, with spatially and temporally stable spectral characteristics, in order to evaluate CASI radiance values against those measured simultaneously at the ground. The following conclusions were reached:

1) A single low altitude flight was sufficient to validate those bands in which the atmospheric effect was least (Default Vegetation Bandset 4 to 6, 670-710nm).

2) The multi-height method was very effective for validating those bands in which scattering dominated (Default Vegetation Bandset 1-3, 450-550 nm).

3) An early morning flight is not ideal due to the rapidly varying solar elevation angle, but the time-dependent spectral correction used in this study was effective in taking account of this.

4) Whilst direct *measurement* of spectral radiance at the ground is possible, it may be more practical in operational terms to *estimate* the spectral radiance from target reflectance and spectral irradiance measured at the time of the flight.

5) The methods used in this research were less successful in validating the CASI radiance in the water absorption band (Band 13, 940nm) and the oxygen absorption band (Band 9, 762nm).

By combining the three approaches used in this research, it would be possible to validate the absolute radiometric calibration of the CASI to better than 5% in all bands except Band 9 (762nm), and better than 3% in bands 1 to 6. This compares with an uncertainty of 1-2% for laboratory radiance calibration for the visible (VIS) wavelength bands.

Further refinement of the methods could lead to an operational procedure of in-flight calibration validation which would remove the need for a mid-season laboratory calibration, reducing disruption to the flight programme, in addition to offering other advantages.

5. Acknowledgements

The authors wish to thank the staff and flight crew of the NERC ARSF for the image data and the Minstry of Defence for allowing access to the Thorney Island site. We are grateful to Bill Damon, Eloise Peters, Michael Riedmann and Nick Hamm for assistance collecting the ground data.

6. References

Abdou, W., Conel, J., Pilorz, S., Helmlinger, M., Bruegge, C., Gaitley, B., Ledeboer, W. and Martonchik, J., 2001. Vicarious calibration. A reflectance-based experiment with AirMISR, *Remote Sensing of Environment* **77,** 338–353.

Arai, K. (2001). A reflectance based vicarious calibration with on-site instruments monitoring, *Advances in Space Research* **28(1),** 11–20.

Bruegge, C., Chrien, N. and Haner, D., 2001. A spectralon BRF database for MISR calibration applications, *Remote Sensing of Environment* **76,** 354–366.

Choi, K.Y. and Milton, E.J., 2002. Standardisation of data from the CASI Incident Light Sensor: A model-based approach designed for operational applications. Proceedings of NERC EPFS Meeting '*Field Spectral Measurements in Remote Sensing' , University of Southampton, 15-16 April 2002, NERC EPFS, CD ROM*.

Dinguirard, M. and Slater, P., 1999. Calibration of Space-multispectral imaging sensors: a review, *Remote Sensing of Environment* **68,** 194–205.

Ferrier, G., 1999. Application of Imaging Spectrometer Data in Identifying Environmental Pollution Caused by Mining at Rodaquilar, Spain, *Remote Sensing of Environment* **68(2),** 125-137.

Karpouzli, E. and Malthus, T., 2003. The empirical line method for the atmospheric correction of IKONOS imagery, *International Journal of Remote Sensing* **24(5),** 1143–1150.

Kieffer, H. and Wildey, R., 1996. Establishing the moon as a spectral radiance standard, *Journal of Atmospheric and Ocean Technology* **13,** 360–375.

Lawless, K.P., Milton, E.J., and Anger, C.M., 1998. Investigation of changes in the reflectance of ground calibration targets (asphalt and concrete), *Information for Sustainability: Proceedings of the 27th International Symposium on Remote Sensing of Environment*, Tromso, Norway, 1-5.

Milton, E.J., Smith, G.M., and Lawless, K.P., 1996. Preparatory research to develop an operational method to calibrate airborne sensor data using a network of ground calibration sites, *Proceedings of the Second International Airborne Remote Sensing Conference and Exhibition*, San Francisco, California, USA, ERIM, Ann Arbor, MI.

Moran, M., Bryant, R., Thome, K., Ni, W., Nouvellon, Y., Gonzalez-Dugo, M., Qi, J. and Clarke, T., 2001. A refined empirical line approach for reflectance factor retrieval from Landsat-5 TM and Landsat-7 ETM+, *Remote Sensing of Environment* **78,** 71–82.

Riedmann, M. and Rollin, E.M., 2000. *Laboratory Calibration Procedure of the Compact Airborne Spectrographic Imager (**casi-2**) owned by NERC*. NERC EPFS, University of Southampton, UK. http://www.soton.ac.uk/~epfs/resources/pdf_pubs/casi_calib.pdf, accessed 12th March 2003.

Rigollier, C., Lefevre, M., Blanc, P. and Wald, L., 2002. The operational calibration of images taken in the visible channel of the Meteosat series of satellites, *Journal of Atmospheric and Ocean Technology,* 19, 1285–1293.

Schott, J., 1997. Remote Sensing - The Image Chain Approach, Oxford University Press, New York.

Schowengerdt, R., 1997. Remote sensing models and methods for image processing, Academic, San Diego.

Secker, J., Staenz, K., Gauthier, R. and Budkewitsch, P., 2001. Vicarious calibration of airborne hyperspectral sensors in operational environments, *Remote Sensing of Environment* **76,** 81–92.

Slater, P., 1980. Remote Sensing - Optics and Optical Systems, Addison-Wesley, Reading, Massachusetts.

Slater, P., 1985. Radiometric considerations in Remote Sensing, *Proceedings of the IEEE* **73(6),** 997–1011.

Slater, P., Biggar, S., Holm, R., Jackson, R., Mao, Y., Moran, M., Palmer, J. and Yuan, B., 1987. Reflectance- and radiance-based methods for the in-flight calibration of multispectral sensors, *Remote Sensing of Environment* **22,** 11–37.

Slater, P., Biggar, S., Thome, K., Gellman, D. and Spyak, P., 1996. Vicarious radiometric calibrations of EOS sensors, *Journal of Atmospheric and Ocean Technology* **13,** 349–359.

Smith, G. and Milton, E., 1999. Technical Note: The use of the Empirical Line Method to calibrate remotely sensed data to reflectance, *International Journal of Remote Sensing* **20(13),** 2653–2662.

Steven, M.D., and Rollin, E.M., 1986. Estimation of atmospheric corrections from multiple aircraft imagery. *International Journal of Remote Sensing*, **7**, 481-497.

Thomas, V., Treitz, P., Jelinski, D., Miller, J., Lafleur, P., McCaughey, J.H., 2003. Image classification of a northern peatland complex using spectral and plant community data, *Remote Sensing of Environment* **84(1),** 83-99.

Thome, K., 2001. Absolute radiometric calibration of Landsat 7 ETM+ using the reflectance-based method, *Remote Sensing of Environment***, 78**, 27–38.